

# Methane projections from Canada’s oil sands tailings using scientific deep learning reveal significant underestimation

Esha Saha<sup>1,2,a</sup>, Oscar Wang<sup>1,2,3</sup>, Amit K. Chakraborty<sup>1,2</sup>, Pablo Venegas Garcia<sup>1,2</sup>, Russell Milne<sup>1,2</sup>, and Hao Wang<sup>1,2,a</sup>

<sup>1</sup>Interdisciplinary Lab for Mathematical Ecology and Epidemiology (ILMEE), University of Alberta, Edmonton (AB), T6G 2J5, Canada

<sup>2</sup>The Department of Mathematical and Statistical Sciences, University of Alberta, Edmonton (AB), T6G 2J5, Canada

<sup>3</sup>The Department of Mathematics and Computer Science, University of Richmond, Richmond (VA), 23173, United States

<sup>a</sup>Corresponding authors. E-mail: esaha1@ualberta.ca, hao8@ualberta.ca

## Abstract

Bitumen extraction for the production of synthetic crude oil in Canada’s Athabasca Oil Sands industry has recently come under spotlight for being a significant source of greenhouse gas emission. A major cause of concern is methane, a greenhouse gas produced by the anaerobic biodegradation of hydrocarbons in oil sands residues, or tailings, stored in settle basins commonly known as oil sands tailing ponds. In order to determine the methane emitting potential of these tailing ponds and have future methane projections, we use real-time weather data, mechanistic models developed from laboratory controlled experiments, and industrial reports to train a physics constrained machine learning model. Our trained model can successfully identify the directions of active ponds and estimate their emission levels, which are generally hard to obtain due to data sampling restrictions. We found that each active oil sands tailing pond could emit between 950 to 1500 tonnes of methane per year, whose environmental impact is equivalent to carbon dioxide emissions from at least 6000 gasoline powered vehicles. Although abandoned ponds are often presumed to have insignificant emissions, our findings indicate that these ponds could become active over time and potentially emit up to 1000 tonnes of methane each year. Taking an average over all datasets that was used in model training, we estimate that emissions around major oil sands regions would need to be reduced by approximately 12% over a year, to reduce the average methane concentrations to 2005 levels.

## 1 Introduction

Anthropogenic sources of greenhouse gases (GHGs) are the major drivers of climate change with methane ( $\text{CH}_4$ ) having the second largest share of emissions in the atmosphere after carbon dioxide ( $\text{CO}_2$ ). Although the comparative impact of  $\text{CH}_4$  is 28 times greater than  $\text{CO}_2$  over a 100-year period [50], it has a shorter lifespan of 12 years, which makes  $\text{CH}_4$  mitigation policies a cost-effective short-term approach to combat global warming [32, 14, 45]. Oil sands activities in particular are regarded as significant sources of water and air pollution. The mining and extraction of oil sands is directly associated with deforestation and release of sulfur oxides, nitrogen oxides, hydrocarbons, and fine particulate matter into the atmosphere. The oil sands tailing ponds (OSTPs) contain toxic industrial wastes that can leak into fresh water sources affecting aquatic ecosystems. Moreover, OSTPs emit significant quantities of  $\text{CH}_4$  from toxin degradation by anaerobic bacteria [40, 41] leading to elevated levels of  $\text{CH}_4$  in the air that can in turn have adverse health

affects on living communities in the region. Frequent onsite data collection for a detailed understanding of OSTPs is often infeasible due to expensive measurement technology, toxic air quality or permit requirements that are hard to obtain [45].

Current research involves building mechanistic models (MM) of  $\text{CH}_4$  emissions (total mass of  $\text{CH}_4$  released in atmosphere from source in a time interval) from toxin/hydrocarbon degradation by bacteria in OSTPs through controlled laboratory experiments [23, 42, 51]. Since experimental limitations lead to exclusion of many relevant parameters such as temperature, pressure, wind speed, etc., MMs cannot be used to accurately assess air quality through concentration levels (the amount of  $\text{CH}_4$  in the air at a given place and time). The relationship between emissions and concentrations can be better described by atmospheric dispersion models (ADMs) [44, 49, 7, 12, 31]. However, simple models like the Gaussian plume or puff models [1, 30] are too unrealistic, while the realistic formulations of ADMs are often too complex to understand and are only feasible to be implemented through industrial softwares such as AEROMOD, CALPUFF, etc [8, 46, 47, 39]. Canada’s 2030 Emissions Reduction Plan aims to reduce carbon-related emissions by 40-45% below 2005 levels by 2030 [13]. Although current reports suggest that the emissions have reduced by 8% below 2005 levels [20], methane concentrations in the Athabasca Oil Sands regions are significantly over 2005 levels. In this work, we conduct a thorough assessment of the air-quality-related effects from different levels of  $\text{CH}_4$  emissions from tailing ponds using scientific machine learning framework.

Data-driven techniques offer a cost-effective and powerful alternative to classical modeling. Some well-known machine learning architectures used for analyzing and predicting air quality include Random Forests (RFs), recurrent neural networks (RNNs), long short-term memory (LSTM), bidirectional LSTM, stacked LSTM, and gated recurrent unit (GRU) [54, 17, 48, 27, 19, 24, 29, 25]. Other data-driven methods use satellite images as an effective way to build a dataset for the purpose of training classifiers to identify active OSTPs so that only high risk ponds may be closely monitored [57, 53, 33]. Machine learning models can also be trained for effective risk prediction of OSTPs as an alternative to standard monitoring systems, which are often expensive and have poor lighting protection abilities [56]. While most existing models (both mechanistic and data-driven) can perform well on estimating emissions from tailing ponds or predicting concentrations, none of them explicitly connect the two quantities to assess the extent to which emission levels could affect quality of air. Thus, we are motivated to build a framework that can successfully use dynamics of tailing ponds emissions to predict concentrations in the atmosphere by preserving the physics of  $\text{CH}_4$  dispersion in air derived from ADMs.

We are particularly interested in the Athabasca Oil Sands, located in northeastern Alberta, Canada which has one of the world’s largest and advanced oil sands industry containing open pits, refining complexes, OSTPs, end-pit-lakes (EPLs), in-situ facilities and various other mining operations. Located in the heart of this region is the the Regional Municipality of Wood Buffalo (RMWB), which contains a mixture of boreal forest, lakes, farmland, urban environments, and industrial complexes. The region contains multiple weather monitoring stations (some located near the oil sands mining areas) under the Wood Buffalo Environmental Association (WBEA) [52] that takes hourly measurements of the ambient air quality and meteorological parameters. Out of more than twenty weather monitoring stations, we are interested in the ones located in a close proximity (within 4 km) from active tailing ponds, measure  $\text{CH}_4$ , and are not surrounded by significant wetlands (which could also emit  $\text{CH}_4$  thus interfering with  $\text{CH}_4$  measurements from the tailing pond as a source). Our stations of interest are Mannix (active OSTP ‘Pond 2/3’ owned by Suncor located approximately 1.4 kilometers (kms) northwest of the station), Lower Camp (active OSTP ‘Pond 2/3’ approximately distance of 3.5 kms southwest of the station and an abandoned OSTP ‘Pond 5’ approximately at 1.4 kms, both owned by Suncor), Mildred Lake (active OSTP ‘Mildred Lake Settling Basin’/MLSB approximately 1.7 kms northwest of the station, owned by Syncrude, and inactive ‘Pond 5’ approximately 2.1 kms owned by Suncor) and Buffalo (nearest pond, ‘West-In-Pit’/WIP presently converted to an EPL at a distance of 0.8 kms northwest of the station). The map of the region is given in Figure 2. Our goal is to use input data from various sources (lab experiments and meteorological parameters) to learn the non-linear relationships between them and predict dispersion of  $\text{CH}_4$  emissions from OSTPs. The trained model can successfully identify and predict emissions and the expected  $\text{CH}_4$  concentration levels at the nearest weather station. We also give an estimate of how much emissions need to be reduced in order to have an air quality comparable

to 2005 levels with respect to methane concentrations.

## 2 Problem Setup and Mathematical Formulation

Mathematically, the goal of the proposed research is to train a parameterized model to track OSTPs using CH<sub>4</sub> concentrations and predict the CH<sub>4</sub> levels in the region. To optimize the weights and biases of our model, the physics constrained optimization problem [55, 21, 16, 36, 22, 6] is modified to include information from MMs as well as real-time data affecting concentrations. For each  $i$ th observations in the set  $\mathcal{I}_{obs}$ , suppose  $\mathbf{x}_i$  denotes the  $(d + 1)$ -dimensional input vector and  $u_i$  denotes observed output. Then given a fixed function  $q : \mathbb{R}^{d+1} \rightarrow \mathbb{R}$  describing emission dynamics (from MMs), our modified constrained optimization problem aims to find a function  $u : \mathbb{R}^{d+1} \rightarrow \mathbb{R}$  by solving the problem,

$$\min_{\phi} \frac{1}{|\mathcal{I}_{obs}|} \sum_{i \in \mathcal{I}_{obs}} (u(\mathbf{x}_i) - u_i)^2 \text{ subject to } F(\phi(\mathbf{x}, u), u, q) = 0, \quad (1)$$

where  $F$  is the physical constraint with unknown function  $\phi$ . Since we want to learn  $u$  from given measurements and  $\phi$  is unknown, we parameterize them with  $u_{\bar{\Theta}}(\mathbf{x})$  and  $\phi_{\hat{\Theta}}(\mathbf{x}, u)$ , respectively where  $\bar{\Theta}$  and  $\hat{\Theta}$  denote the unknown parameters to be learned through training. Different function representation models such as sparse polynomial approximation [2, 11, 38], random feature models [34, 18, 37], or neural networks [28] may be used. Converting Eq. (1) to an unconstrained optimization problem we get,

$$\min_{\bar{\Theta}, \hat{\Theta}} \frac{1}{|\mathcal{I}_{obs}|} \sum_{i \in \mathcal{I}_{obs}} \left[ (u_{\bar{\Theta}}(\mathbf{x}_i) - u_i)^2 + \lambda (F(\phi_{\hat{\Theta}}(\mathbf{x}_i, u_{\bar{\Theta}}), u_{\bar{\Theta}}, q(\mathbf{x}_i)))^2 \right], \quad (2)$$

where  $\lambda \in (0, \infty)$ . An advantage of using this method (also known as penalty method) is that it avoids solving the constraint  $F(\phi, u, q) = 0$  [55]. However, the physical constraints may not be satisfied exactly i.e., theoretically,  $F(\phi, u, q) = 0$  will hold only when  $\lambda \rightarrow \infty$  [55]. The value of  $\lambda$  defines the magnitude of cost for violating the constraint. The minimization of the above penalized loss in Eq. (2) will give a solution with small value of the regularization term defined on the physical constraint  $F$ . While optimizing the choice of  $\lambda$ , it is important to remember that a large value of  $\lambda$  places less weight on the objective function. Hence, a proper choice of  $\lambda$  is based on the desirable trade-off between fitting the observed value and satisfying the constraint. This technique has been adapted in numerous works involving learning of systems of PDEs/ODEs from data [21, 35]. Our choice of the constraint  $F$  is derived from one of the atmospheric dispersion models called Gaussian Plume Model (GPM) [44] described through the equation

$$\frac{\partial u}{\partial t} + \nabla \cdot J = q,$$

where  $u(\vec{x}, t)$  is the mass concentration,  $q(\vec{x}, t)$  is a source (or sink) and  $J$  is mass flux due to diffusion ( $J_D$ ) and advection ( $J_A$ ), and  $\vec{x}$  and  $t$  denote space and time respectively. In our framework, we learn the concentration  $u(\vec{x}, t)$  from the methane concentration data measured by the weather station. Assuming negligible sinks, the function  $q$  defined from the MMs, which helps to learn the unknown function  $\nabla \cdot J$ . Since we fix the coordinates of the source (OSTPs) and weather stations in space,  $u$  and  $q$  are independent of spatial coordinates. We are more interested to explore the relationship of these two functions ( $u$  and  $q$ ) to various input variables involving atmospheric parameters and/or hydrocarbon degradation. Given the input dataset  $\mathbf{x} = [\mathbf{x}_{dil}, \mathbf{x}_{atm}, \mathbf{t}]^T \in \mathbb{R}^{d+1}$  (where  $\mathbf{x}_{dil}$  is built from solutions of the MMs and  $\mathbf{x}_{atm}$  is built from the real-time weather station measurements), the methane concentrations and emissions are trained using the parameterization below in Eq. (3) and Eq. (4). Output of the first network  $u_{\bar{\Theta}}$  gives the predicted methane concentration. We then concatenate this output with atmospheric parameters  $\mathbf{x}_{atm}$  since those are the only variables that can potentially affect diffusion/advection, and use it as an input to the second neural network that estimates  $\nabla \cdot J$ . The the exact form of the outputs are given by

$$u_{\bar{\Theta}} = \bar{\Theta}_4 \sigma(\bar{\Theta}_3 \sigma(\bar{\Theta}_2 \sigma(\bar{\Theta}_1 \mathbf{x}))) \quad (3)$$

$$q(\mathbf{x}, t) = \text{Grad}_t(u_{\bar{\Theta}}) + \hat{\Theta}_3 \sigma(\hat{\Theta}_2 \sigma(\hat{\Theta}_1 [u_{\bar{\Theta}}, \mathbf{x}_{atm}])), \quad (4)$$

where  $\sigma$  denotes the activation function and  $\text{Grad}_t(\cdot)$  denotes the partial time derivative of the output  $u_{\bar{\Theta}}$ . Alternatively, the function to define  $\nabla \cdot J$  can also be represented with a known basis such as a polynomial basis. This can be used when trying to decipher the important variables affecting the diffusion/advection terms. Eq. (4) thus modifies to

$$q(\mathbf{x}, t) = \text{Grad}_t(u_{\bar{\Theta}}) + \hat{\Theta}_1 \mathcal{P}([u_{\bar{\Theta}}, \mathbf{x}_{atm}]),$$

where  $\mathcal{P}([z_1, \dots, z_n]) = [1, z_1, \dots, z_n, z_1 z_2, \dots, z_{n-1} z_n, z_1^2, \dots, z_n^2]$ .

In order to estimate source emissions and identify active tailings, we modify the constraint to satisfy reverse dispersion models that aim to quantify emissions when concentrations are given. In the reverse formulation, using inputs  $[\mathbf{x}_{dil}, \mathbf{x}_{atm}, \mathbf{t}]^T \in \mathbb{R}^{d+1}$  we still learn  $u_{\bar{\Theta}}$  from fitting the model to observed concentrations as in Eq. (3), however the constraint is now based finding source emissions  $q$  from

$$(C/Q)_{est} q + u_{bg} = u,$$

where  $u_{bg}$  and  $u$  are background and measured methane concentration levels, respectively and  $(C/Q)_{est}$  is called an influence function (in classical approaches it can be estimated from finite difference approximations of ADMs). The main challenge of the reverse formulation is to find an appropriate representation of the influence function and its inverse for accurate emission estimates. We parameterize the inverse of influence function as a neural network so that the constraint representation in Eq. (4) becomes

$$q(\mathbf{x}, t) = \hat{\Theta}_3 \sigma \left( \hat{\Theta}_2 \sigma \left( \hat{\Theta}_1 [u_{\bar{\Theta}}, \mathbf{x}_{atm}] \right) \right). \quad (5)$$

Note that in this formulation, the term  $C_{bg}$  term is balanced out by the bias terms present in estimating emissions and concentrations. This formulations is particularly beneficial in estimating emissions from different directions around the weather stations. We train the model on our datasets and then in order to get emission estimates, we replace  $u_{\bar{\Theta}}$  in Eq. (3) with the concentration data measured by the weather station into the trained model. The emission estimates per day are then added up to get cumulative emissions over a given year.

### 3 Model Framework

In order to train our model, we require data from two separate but related phenomenon: (i) real-time  $\text{CH}_4$  concentration and atmospheric data from weather monitoring stations; (ii) simulated data from experimentally validated MM, estimating methane emissions and hydrocarbon degradation in active OSTPs. A pictorial representation of the framework is given in Figure 1.

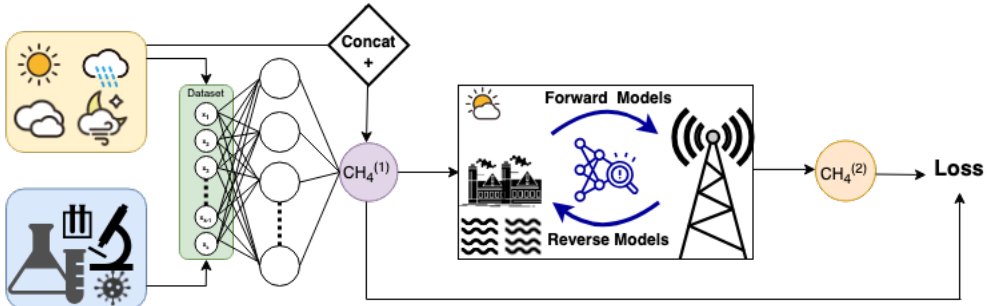


Figure 1: Proposed framework of physics driven learning of atmospheric methane dispersion.

### 3.1 Study Area

Our region of interest is located around the industrial area near Syncrude and Suncor Base Plants. We only consider the OSTPs that are active and have a weather monitoring station measuring methane located close to them. The study area is given in Figure 2.

### 3.2 Data from Real-Time Weather Station Measurements

Dataset for atmospheric parameters and methane concentrations was built from data collected by the Wood Buffalo Environmental Association (WBEA) [52]. Since the MMs are based on experiments on active OSTPs, the training dataset is built only for stations near an active OSTP (MLSB and Pond 2/3 as reported in [9]). We pick the stations in a close proximity to these active OSTPs that have no other methane sources (for example, wetlands) between them. For each station, we build the dataset by filtering observations with wind direction ranges based on location of active OSTPs i.e., Mannix (300-320 degrees), Lower Camp (160-180 degrees), and Mildred Lake (300-340 degrees). We average and interpolate (using spline interpolation of order one) the data as required so that the final dataset contains daily observation. The map of the weather stations and OSTPs are given in Figure 2.

### 3.3 Data Simulated from Mechanistic Models of OSTPs

To build dataset corresponding to hydrocarbon degradation and methane emissions from OSTPs, we use MMs developed by studying the properties and dynamics of methane production in OSTPs through controlled lab experiments [23, 42, 51]. These models are developed by considering the most labile hydrocarbons present in the solvents used by each of the oil sands companies. The models are generally represented by a dynamical system whose general form can be written as described in Eq. (6). The system describes the degradation dynamics of each of the labile hydrocarbon by methanogenic bacteria. For each fixed  $i$ , the system of



Figure 2: Map depicting region of interest along with the main weather stations and OSTPs/EPLs.

equations are given as

$$\begin{aligned}
 \frac{dC_i}{dt} &= f(C_i, t, y_1, \dots, y_k) \\
 \frac{dy_j}{dt} &= g_j(C_i, t, y_j) \text{ for } j = 1, \dots, k \\
 \text{CH}_4 &= h(C_i, y_1, \dots, y_k, \mu_i, t)
 \end{aligned}
 \tag{6}$$

where  $C_i$  denotes each of the hydrocarbons,  $y_j$  denotes other variables in consideration (for example, other nutrients, biomass of microbes, etc) and  $\mu_i$  denotes the set of constants corresponding to methane production (for example, microbial efficacy, stoichiometric factor, etc). The exact nature of the functions  $f, g$  and  $h$  along with the other parameters can be found in prior works on modelling methane emissions from OSTPs [23, 42, 51].

For each company, we use the monthly ‘Flared and Wasted’ category of “diluent” from [4] as the total monthly inflow of hydrocarbons into the ponds. These hydrocarbons are subsequently used up by methanogenic bacteria leading to methane emissions. Since the reported diluents includes all the OSTPs under the ownership of a company, we use the fine fluid tailings (FFT) volume percentage of each active lake from [3] to get an estimate of the fraction of diluents in each lake. A constant daily inflow of diluents is assumed i.e. the total monthly diluent reported in [4] is divided equally by the number of days in the month. The system is solved with a timestep of one day for a month. This is done for all the months from January 2020 to December 2023 in order to build the dataset. This approach is similar to the technique followed in [51]. We also experimented with datasets built based on another methanogenesis models [23]. Note that when generating the data using the model proposed in [23], we identified a small number of generated daily values (about 1% of values) that were not biologically realistic. We considered these values to be numerical artifacts of simulation driven by the stiffness of the model, and hence replaced each one with the generated value for the day before it for the sake of simplicity and biological fidelity. The results and conclusions for the both the models were the same, and thus we present the results for only datasets built using [51].

### 3.4 Model Framework and Training

In developing the framework, we use the fact that hydrocarbons in tailings ponds directly affect emissions which in turn affects concentrations. Majority of the atmospheric variables have no effect on hydrocarbon degradation since the process takes place deep in the OSTPs. However, once emissions start interacting with atmospheric variables, they can directly affect concentrations. The model considers three types of input data: (i)  $\mathbf{x}_{dil}$  denoting the degradation of hydrocarbons in OSTPs and obtained from solving MMs in literature; (ii)  $\mathbf{x}_{atm}$  representing atmospheric parameters such as ambient temperature, wind speed, wind direction, solar activity, etc; and (iii) time vector  $\mathbf{t}$ . These three inputs  $\mathbf{x}_{dil}$ ,  $\mathbf{x}_{atm}$ , and  $\mathbf{t}$  together form the input  $\mathbf{x}$  and are used to define the minimization problem. The pseudocode for implementing our model is given in Algorithm 1. While the proposed method can be combined with any machine learning architecture and constraints, we proposed three general formulations of our model, each with its own advantages and applications (see Section 2). Table 1 gives all the variations as well as some other models that were used for comparison. The pseudocode for model training is given in Algorithm 1. The entire dataset contains 1096 daily measurements dated between January 1, 2020 to December 31, 2022. We standardize the entire dataset between 0 and 1 to avoid unnecessary bias of input features with a larger scale. Given the size of our dataset, we use three layers with 500 and 200 neurons in all our experiments to learn  $u_{\bar{\Theta}}$  and  $\phi_{\bar{\Theta}}$ , respectively. For optimizing the weights, we use a stochastic gradient descent (SGD) algorithm with 10,000 iterations, learning rate optimized between  $10^{-2}$  and  $10^{-3}$ , and momentum 0.9. Since the data from weather monitoring stations are noisy, we use an  $\ell_2$  based weight decay parameter of  $10^{-3}$  in the SGD algorithm to avoid overfitting. The model training was done on 80% of the data and validation on the last 20% of the dataset. Dataset created for the year 2023 served as a test set which was used to test our model’s long term predictive capabilities based on training on historical data. For 10 random initializations, we train the model and calculate the estimated emissions using real concentration data for the years 2020 and 2021 (true

Model name	Formula	Constrained
Ours <sub>Forward</sub>	$\text{CH}_4^{(1)} = \bar{\Theta}_4 \sigma (\bar{\Theta}_3 \sigma (\bar{\Theta}_2 \sigma (\bar{\Theta}_1 \mathbf{x})))$ $\text{CH}_4^{(2)} = \text{Grad}_t \left( \text{CH}_4^{(1)} \right) + \hat{\Theta}_3 \sigma \left( \hat{\Theta}_2 \sigma \left( \hat{\Theta}_1 \left[ \text{CH}_4^{(1)}, \mathbf{x}_{atm} \right] \right) \right)$	✓
Ours <sub>Reverse</sub>	$\text{CH}_4^{(1)} = \bar{\Theta}_3 \sigma (\bar{\Theta}_2 \sigma (\bar{\Theta}_1 \mathbf{x}))$ $\text{CH}_4^{(2)} = \hat{\Theta}_3 \sigma \left( \hat{\Theta}_2 \sigma \left( \hat{\Theta}_1 \left[ \text{CH}_4^{(1)}, \mathbf{x}_{atm} \right] \right) \right)$	✓
Ours <sub>Poly</sub>	$\text{CH}_4^{(1)} = \bar{\Theta}_4 \sigma (\bar{\Theta}_3 \sigma (\bar{\Theta}_2 \sigma (\bar{\Theta}_1 \mathbf{x})))$ $\text{CH}_4^{(2)} = \text{Grad}_t \left( \text{CH}_4^{(1)} \right) + \hat{\Theta}_1 \mathcal{P} \left( \left[ \text{CH}_4^{(1)}, \mathbf{x}_{atm} \right] \right)$	✓
RNN <sub>mod</sub>	$\text{CH}_4^{(1)} = \bar{\Theta}_4 \sigma (\bar{\Theta}_3 \sigma (\bar{\Theta}_2 \sigma (\bar{\Theta}_1 \mathbf{x})))$ $\text{CH}_4^{(2)} = \hat{\Theta}_3 \sigma \left( \hat{\Theta}_2 \sigma \left( \hat{\Theta}_1 \text{CH}_4^{(1)} \right) \right)$	✓
NN	$\begin{bmatrix} \text{CH}_4^{(1)} \\ \text{CH}_4^{(2)} \end{bmatrix} = \Theta_5 \sigma (\Theta_4 \sigma (\Theta_3 \sigma (\Theta_2 \sigma (\Theta_1 \mathbf{x}))))$	✗
LSTM	$\begin{bmatrix} \text{CH}_4^{(1)} \\ \text{CH}_4^{(2)} \end{bmatrix} = \text{LSTM}(\mathbf{x})$	✗

Table 1: Different models used for comparing predictions of methane emissions and concentrations.

emission data from companies was only available for these two years). The model whose cumulative CH<sub>4</sub> estimations are closest to the true emissions as reported in official documents was picked for further analysis.

---

**Algorithm 1** Model training using CHAMP

---

**Input:** Pre-processed and interpolated input data  $\mathbf{x} = [\mathbf{x}_{dil}, \mathbf{x}_{atm}, \mathbf{t}]$ , observed data  $u$ , emission function  $q(\mathbf{x})$ , observations indices set  $\mathcal{I}_{obs}$ , physical constraint  $F$ , model architectures for learning  $u_{\bar{\Theta}}$  and  $\phi_{\bar{\Theta}}$ , penalty parameter  $\lambda$ , total epochs `epoch`.

**Algorithm:**

- 1: **for**  $j$  in epochs **do**
- 2:      $y = u_{\bar{\Theta}}(\mathbf{x})$ .
- 3:      $z = \phi_{\bar{\Theta}}(y, \mathbf{x}_{atm})$
- 4:     Update  $\Theta = [\bar{\Theta}, \hat{\Theta}]$  by minimizing the loss,

$$\frac{1}{|\mathcal{I}_{obs}|} \|y - u\|_2^2 + \frac{\lambda}{|\mathcal{I}_{obs}|} \|F(z, y, q)\|_2^2$$

- 5:     **if** Sparse Parameters == True **then**
- 6:         **for**  $k$  in size( $\hat{\Theta}$ ) **do**
- 7:             **if**  $|\hat{\Theta}_k| < 10^{-4}$  **then**
- 8:                  $\hat{\Theta}_k = 0$
- 9:             **end if**
- 10:         **end for**
- 11:     **end if**
- 12: **end for**

**Output:** Concentrations  $y$  and emissions  $z$

---

	Concentration			Emission		
	Mannix	LC	ML	Mannix	LC	ML
Ours <sub>Forward</sub>	0.5425	<b>0.3101</b>	0.5814	0.0992	0.1615	0.0517
Ours <sub>Reverse</sub>	0.6566	0.4301	0.5702	0.1085	0.1369	0.0543
Ours <sub>Poly</sub>	<b>0.4624</b>	0.3140	<b>0.4225</b>	0.5380	0.1977	0.0942
RNN <sub>mod</sub>	0.6239	0.4314	2.1859	0.0661	0.0737	0.7127
NN	0.5683	0.3132	0.4618	<b>0.0721</b>	<b>0.0754</b>	<b>0.0187</b>
LSTM	0.6454	0.3914	0.5550	0.2426	0.2568	0.0711

Table 2: Average of relative training and validation errors for predicting concentrations and emissions from each station and its corresponding tailing pond. For each column (station), the lowest error is highlighted.

## 4 Results

We discuss the outcomes of our model’s simulations with respect to three objectives: (i) forecasting methane emissions and concentrations from tailing ponds jointly; (ii) identifying the active tailing ponds around weather stations; (iii) estimating target emissions for improving air quality. Out of the four stations selected based on their proximity to OSTPs (or EPLs), we build datasets using the stations that capture CH<sub>4</sub> from ‘active’ OSTPs. We classify an OSTP to be ‘active’ if there is continuous inflow of diluents (industrial residues). For training, only the data of weather stations that are close to an active pond are used because the source estimations using MMs are based on experiments modeled after active OSTPs. Based on available data and information on OSTPs, we select stations Mannix with Pond 2/3, Lower Camp with Pond 2/3 and Mildred Lake with MLSB for building the dataset. The model performance was assessed using two criteria: (i) average of the relative  $\ell_2$  error on training and validation set; (ii) plots of true and predicted outputs. The relative error is computed for both concentrations and emissions. The formula for computing the relative error ( $RE$ ) is given by

$$RE(y_{true}, y_{pred}) = \frac{\|y_{true} - y_{pred}\|_2}{\|y_{true}\|_2} \quad (7)$$

where  $y_{true}$  and  $y_{pred}$  denote the true and predicted outputs, respectively. The two-fold assessment of using both relative errors and plots helps us to compare how well each method can generalize the data on unseen data, especially in cases when their errors are comparable. The table of relative errors is given in Table 2.

### 4.1 Forecasting Methane from Tailing Ponds

Given the mass of industrial waste in a selected OSTP and the meteorological conditions around them, our model is trained to predict CH<sub>4</sub> emissions from the pond and the corresponding concentration in air measured by the closest weather monitoring station. The model learns the unknown dispersion/advection terms in the ADM, which can be learned using different representations, such as using fully-connected neural networks, polynomial representation, Fourier basis representation, etc. We compare a three layer neural network and a polynomial representation of order two with a hard thresholding induced sparsity for learning the dispersion/advection terms.

**Mannix:** All the variants of the proposed model (forward, reverse and poly) successfully learn the trends of the true concentrations as well as simulated emissions from given MM as depicted in Figure 3. From Table 2, we see that forward or polynomial representations have the lowest error for predicting concentrations outperforming all other models. On the other hand for emissions, since the concentration data is noisy, we also see certain noise/oscillations present in the emission predictions. The neural network representation performs well in predicting both the quantities of interest. The results from RNN<sub>mod</sub> model shows that it can learn the trend of the concentration data due to it being trained as a constrained optimization problem. The model learns certain dependencies between the two output quantities. However, excluding



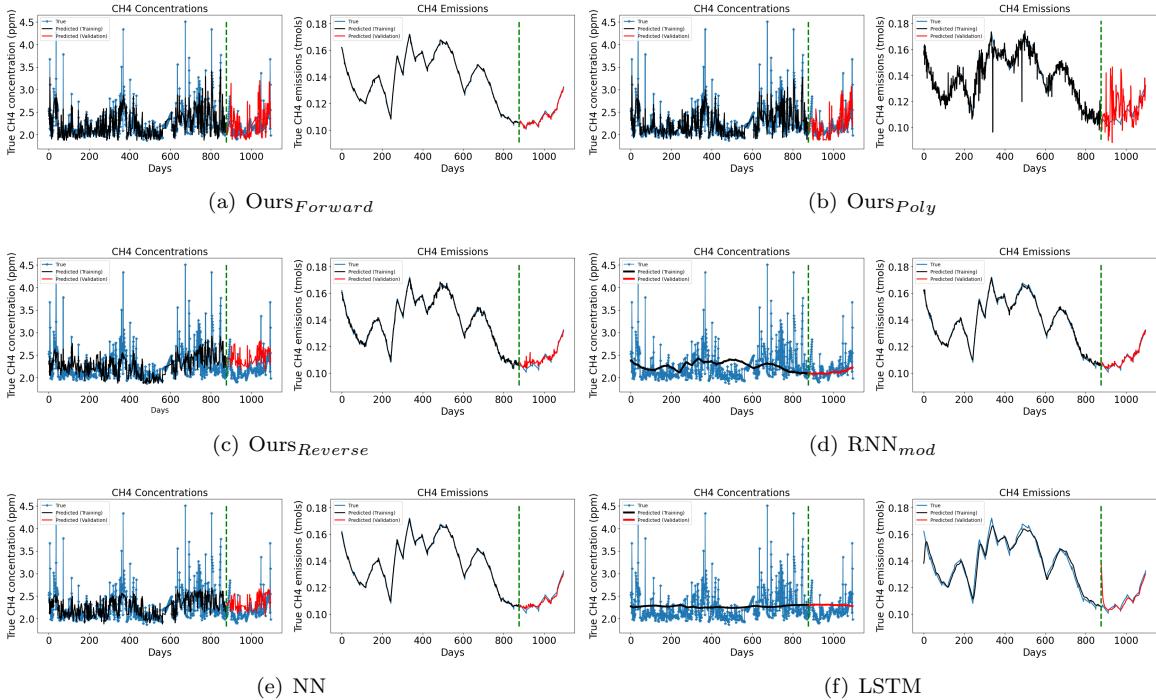


Figure 3: Results for weather station Mannix in predicting  $\text{CH}_4$  concentrations and emissions. The green dashed line indicates the data split between training and validation set.

$x_{atm}$  from the constraint leads to the model not learning the variations caused by atmospheric parameters in the concentration data. For the other methods that are trained without any physical constraints, we see that the full NN model performs comparable to the proposed model (see Figure 3). It learns the trends of methane concentrations and a smooth curve for the methane emission data as simulated by the MMs contributing to the lowest relative error for emissions (see Table 2). However, this model is equivalent to combining two separate models for learning concentrations and emissions and does not capture dependencies between the two outputs. The LSTM model fails to learn anything from the concentration data, but can easily learn the emission data given that it is simulated from MM as depicted in Figure 3.

**Lower Camp:** As in the previous case, the our models and NN perform the best for concentration predictions. For MM based emission simulations, the NN learns the smooth functions describing emissions, while the our models learn the trend of emissions with some oscillations directly connected to concentration trends. The  $\text{RNN}_{mod}$  model fails to learn the concentration data due to absence of any atmospheric parameters in defining the constraint and the LSTM model just learns a straight line that through the concentration dataset (see Figure 4). For learning the emission data, all the models learn it well since it is simulated from a known MM.

**Mildred Lake:** From Figure 5, we see the our models best fit the concentration data with lowest error given by polynomial fitted model (see Table 2). This is closely followed by the NN model. Comparing, we see that the our trained models are much better at fitting well with majority of the peaks on concentration data (except the extremely sharp one beyond 2.5 parts per million (ppm) as they are considered as outliers in the dataset) than the NN model. The  $\text{RNN}_{mod}$  model can only pickup the trend of concentration data while fitting almost perfectly with the emission data. The LSTM model simply fails to generalize anything in the concentration data. For emission data, the trends are similar to the previous stations where the unconstrained formulations (NN and LSTM) learn the smooth function almost perfectly.

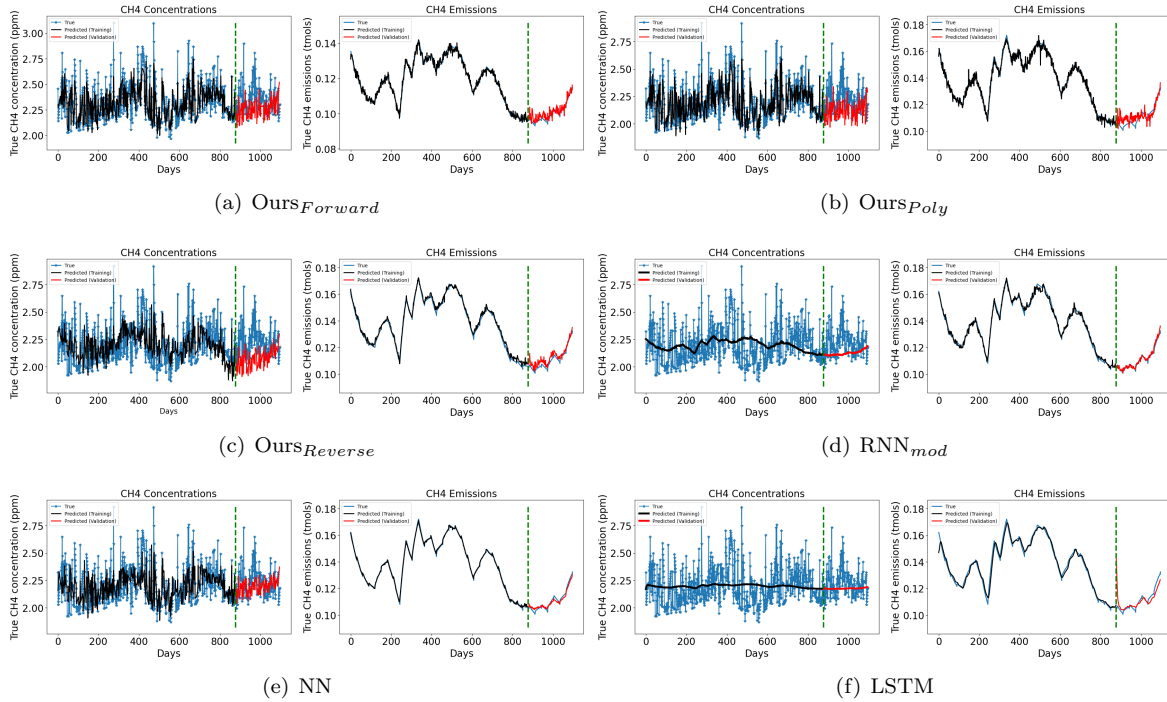


Figure 4: Results for weather station Lower Camp in predicting CH<sub>4</sub> concentrations and emissions. The green dashed line indicates the data split between training and validation set.

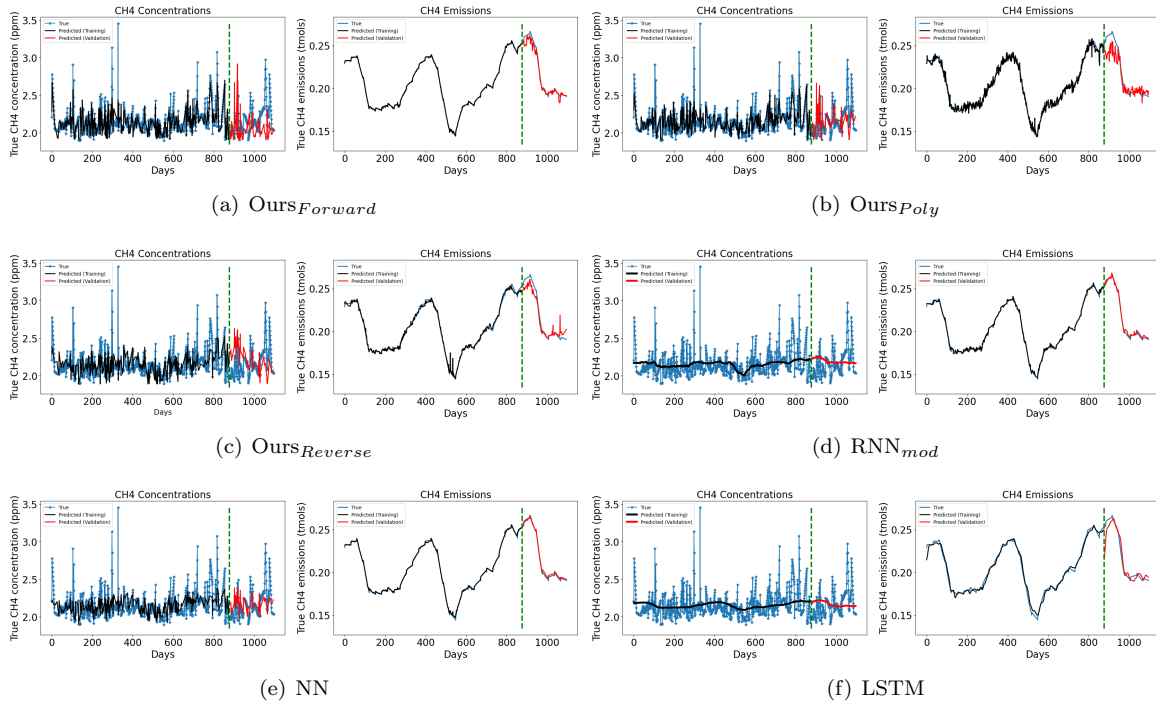


Figure 5: Results for weather station Mildred Lake in predicting CH<sub>4</sub> concentrations and emissions. The green dashed line indicates the data split between training and validation set.

To test our model’s capacity to predict long term methane concentrations, we obtain model predictions for the year 2023 using the neural network representation of ADM model and compare it with the observed data. The plots given in Figure 6 show that the trained model accurately estimates emissions from OSTPs upto one year ahead based on the meteorological data and mass of expected amount of diluents (industrial waste) in the ponds. For the concentrations, the model can suggest future trends, preserving exact values for observations close to the average  $\text{CH}_4$  values. However, the variation is larger (for higher recorded observation) since the real-time data is noisy and the model ignores extreme large values as outliers. Overall, we can conclude that our model either performs comparable or outperforms all other alternative models in long-terms projections of  $\text{CH}_4$ .

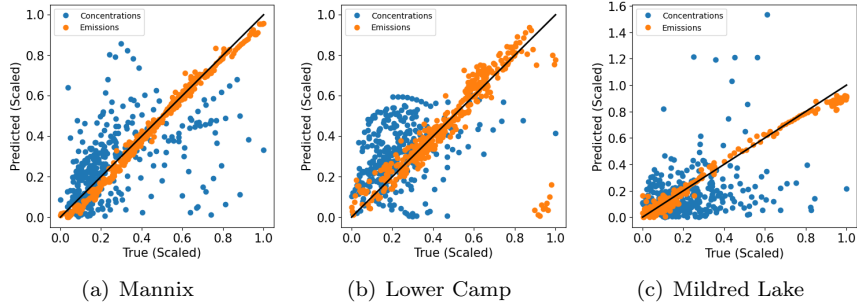


Figure 6: Normalized values of true versus predicted  $\text{CH}_4$  concentrations and emissions in 2023 for stations Mannix, Lower Camp and Mildred Lake using a neural network representation of the dispersion/advection terms in the ADM.

## 4.2 Tracking Methane Emitting Sources around Weather Stations

Since all OSTPs cannot be monitored/tracked continuously for  $\text{CH}_4$  emissions, we train a model using the reverse formulation of ADM to estimate daily emissions with wind directions 360 degrees around a selected weather station in the study. Once trained, we replace the input  $u_{\ominus}$  in Eq. (5) with true  $\text{CH}_4$  concentration data from weather monitoring stations to obtain daily emission estimates from the tailing ponds. Daily predicted emissions are then added to obtain cumulative emissions for each year from 2020 to 2023 and is given as a radial plot in Figure 7. The two major reported OSTPs (MLSB and Pond 2/3) and abandoned pond/EPLs (Pond 5 and WIP) are marked on the map. To compare emission levels over a period of three years, we plot the emissions for the year 2020 and 2023 on a map and mark all the reported OSTPs and EPLs near them. For stations in the vicinity of inactive ponds, we used a trained model from another appropriate station to get emission estimates. For example, since WIP lake (an inactive pond) near station Buffalo is owned by Syncrude, we can use the model trained for Mildred Lake with inputs from Buffalo station to get emission estimates around it. For each station we see the estimated emissions are highest from the direction of tailing ponds. Both Mannix and Lower Camp indicate that  $\text{CH}_4$  emissions from Pond 2/3 are more than 850 tonnes per year. Each year, station Mildred Lake captures more than 1200 tonnes of  $\text{CH}_4$  emissions from the direction of MLSB, which is almost 20% more than the reported amounts. The other inactive ponds (WIP and Pond 5) are often ignored as a significant sources of  $\text{CH}_4$  emissions as there is no inflow of diluents. However, using the dataset of station Buffalo, our model estimates more than 1200 tonnes of emissions coming from the the direction of WIP lake and about 950-1000 tonnes of  $\text{CH}_4$  from Pond 5. These significant levels of emissions from Pond 5 can also be cross-verified with the results obtained for stations Lower Camp and Mildred Lake. Note that while the distance of the stations from the tailing ponds can affect the exact estimation of emissions, it is clear from the plots that abandoned ponds are also contributing to emissions.

Upon comparing both the plots for the year 2020 and 2023 in Figure 7, we see that there has been a significant increase in emissions over the three years by at least 100 tonnes in each of the 20 degree

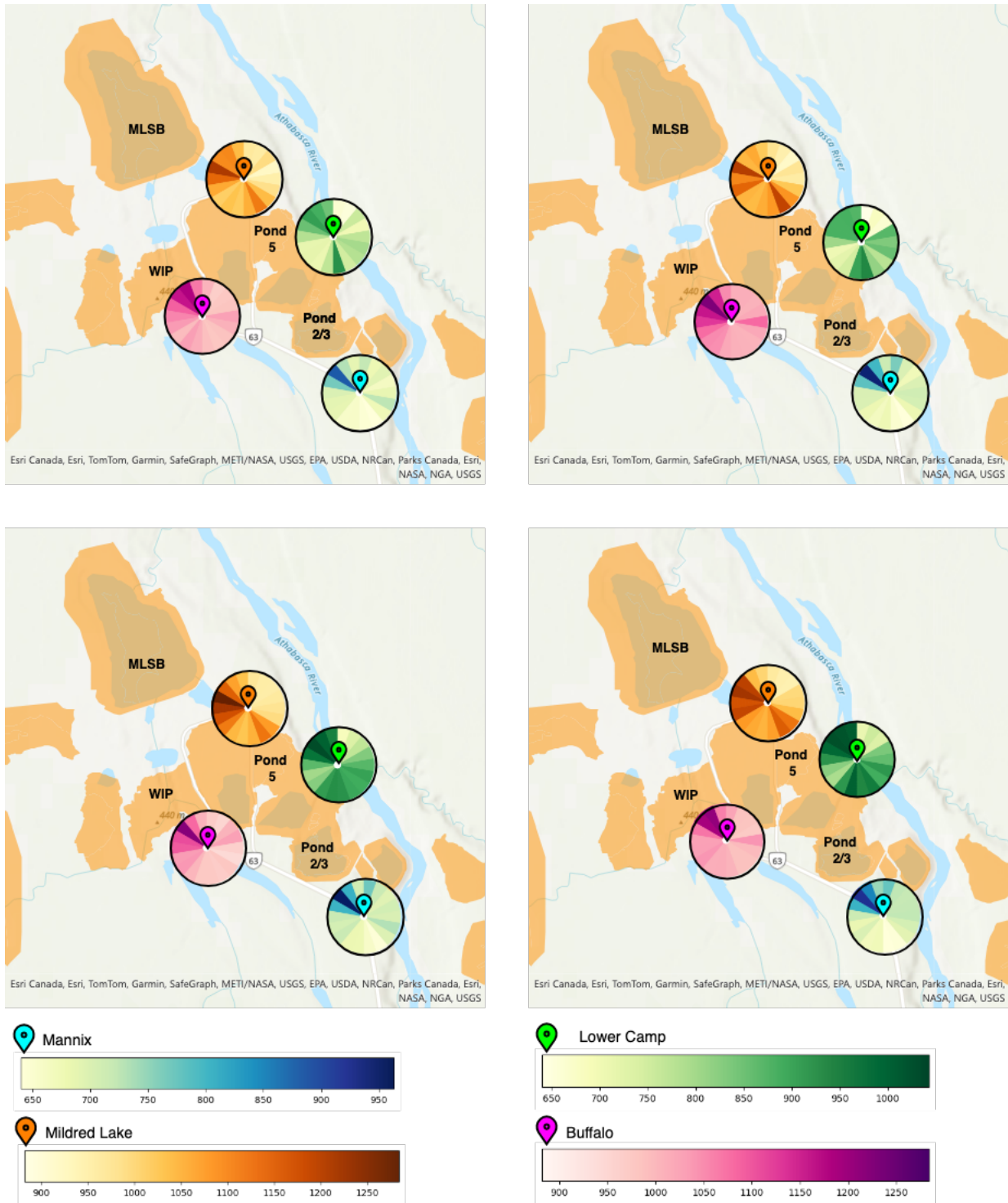


Figure 7: Emissions (in tonnes) per year predicted by our model from around the weather stations in our region of case study over four years. **Top left:** Year 2020. **Top right:** Year 2021, **Bottom left:** Year 2022. **Bottom right:** Year 2023.

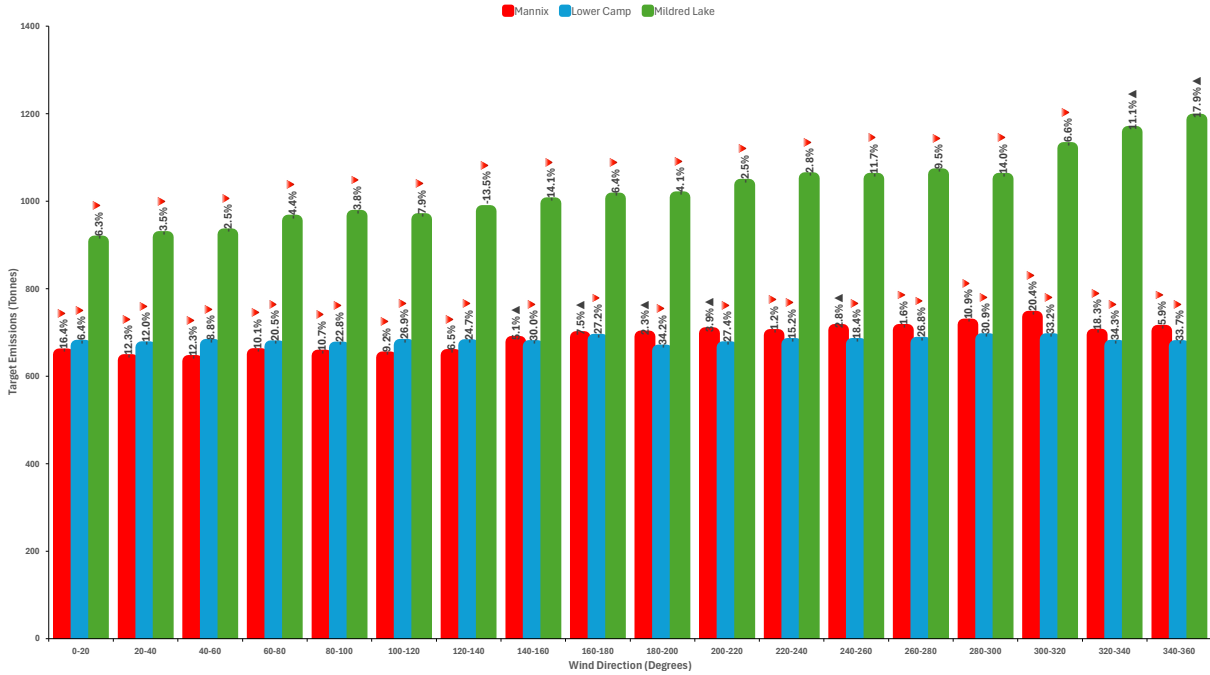


Figure 8: Yearly target emissions from each twenty degree interval wind direction for each weather monitoring station to attain methane concentration average of 1.75 ppm.

wind direction interval near the tailing ponds. Both MLSB and Pond 2/3 have started contributing higher amounts of CH<sub>4</sub>. For year 2023, we also find elevated emissions for both Mannix and Lower Camp with wind directions 20-140 degrees and 60-140 degrees respectively, coming from OSTPs (such as Pond 8 owned by Suncor or similar sources in the area) south-east of the stations across the Athabasca river. Some other directions with lower emission levels of about 700-900 tonnes (West of Mannix, South-East of Buffalo, SW of Lower Camp), all correspond to either in-situ facilities, industrial activity or inactive tailing ponds. For each of the years we see that there is significant emission. We see that in most cases, significantly higher emission rates are found either directly in the direction of the tailing pond or slightly near it within a 20 to 30 degrees of wind direction.

### 4.3 Estimating Levels of Emissions for Better Air Quality

In this section, we quantify how much emissions would have to be reduced from 2023 over one year to reach an average atmospheric methane concentration level of 2005 at 1.75 parts per million (ppm). Considering all other parameters remain same as measured in 2023, for each station, we shift CH<sub>4</sub> concentration data to have a mean of 1.75 ppm (instead of the current mean of more than 2 ppm). We use this dataset into our trained reverse model to estimate the emissions and compare results obtained for 2023 from the previous section. The plot for required emissions to reach 2005 CH<sub>4</sub> concentration levels around each of the three stations is given in Figure 8. Around Mannix, emissions from direction of Pond 2/3 (300-340 degrees) need to be reduced by more than 18% followed by a 16.4% reduction from other smaller ponds around it. The same can also be concluded from Lower Camp, where more than 27% reduction is required from Pond 2/3 and other OSTPs across the Athabasca river (140-220 degrees) for controlling atmospheric CH<sub>4</sub>, in addition to the 30% emissions control needed from Pond 5 and surrounding areas (280 - 360 degrees). Finally for MLSB, future targets need to be about 14% lower in direction of Pond 5 (120-160 degrees) and about 14% in direction of Mildred Lake (280 - 300 degrees). It may be also be interesting to note that oil sands activities in some of the directions can also be expanded to increase emissions by 3% to 20% of current levels.

## 5 Discussion

Atmospheric  $\text{CH}_4$  can be affected by natural as well as anthropogenic factors. Data of  $\text{CH}_4$  concentrations demonstrates oscillatory/seasonal behaviour, whose natural causes are related to atmospheric  $\text{CH}_4$  sinks related to temperature, solar activity, etc. While it is obvious from laboratory experiments that the amount of diluents in the OSTPs directly affects emission rates, the connection between source emissions from OSTPs and atmospheric concentrations is hard to obtain. In order to build a reliable framework, our model was trained by connecting all possible dynamics connected to  $\text{CH}_4$  emissions from OSTPs and the air quality in the region: MM of hydrocarbon degradation [51, 23, 42], ADMs for  $\text{CH}_4$  dispersion [44] and atmospheric data that drives atmospheric diffusion and advection.

The model performances are compared based on both, plots and relative errors. Table 2 shows that for predicting concentrations, either the neural network or sparse polynomial representation of the dispersion/advection terms gives the lowest error which can be attributed to both the methods having similar predictive capabilities [5]. The differences in the model performances are attributed to the weather station used for dataset building i.e., quality and quantity of data available for each station can vary since it gets affected by a number of external factors such as the proximity of OSTPs to the weather stations, height of measurement sensors, etc. For example, if a weather station is located at a higher elevation on a cliff, it is more likely to be affected by high wind speeds [43], thus leading to a noisy dataset. The  $\text{CH}_4$  concentration data collected for station Mannix has the highest variance of 0.12 with maximum and average measurements being 4.56 ppm and 2.21 ppm respectively, followed by station Mildred Lake with a variance of 0.05, maximum and average concentrations are 3.95 ppm and 2.1 ppm respectively. Station Lower Camp has concentration readings with lowest variance at 0.03 with maximum and average  $\text{CH}_4$  measurements being 3.36 ppm and 2.001 ppm respectively. From the table of relative errors (Table 2), it can be seen that a lower the variance improves the performance of the models. This happens as data-driven models tend to have larger biases in predicting the extreme values, especially in data-scarce training regimes such as in this scenario. Superior model performance for the station Lower Camp can also be attributed to its restricted range of wind direction during the dataset building stage, making the input dataset more less noisy in comparison to other stations. Note that since the ponds are owned by different companies, the hydrocarbon degradation dynamics can differ based on the chemical composition of diluents used. Depending on how well the laboratory experiments were able to incorporate this variation from chemical compositions into the MM, a variation in our model training (and hence performance) can be expected. The relative errors for predicting  $\text{CH}_4$  emissions is less than 0.2 for all the models. Since the NN model’s training is equivalent to learning both the quantities (concentrations and emissions) independently from their respective inputs, its relative error is the lowest. Thus, the NN model might be a better option if we only are interested in emission prediction from diluent data. However, it cannot be used to find complex dependencies between the atmospheric and diluent parameters nor used to trace sources of emissions. This happens because the input to the model includes both atmospheric parameters (see Eq. (4), and Eq. (5)) that are noisy. For the proposed physics-constrained model(s), although emission predictions are slightly noisy, it does not affect the generalization power of our trained model as it can still preserve the overall trends on unseen data for both the quantities.

In the reverse formulation of the model, we use the trained model to trace the emissions from all the direction around each weather monitoring station. We use the second part of the trained model by considering the real concentration data along with the weather parameters to track emissions and possible sources (replace the input  $u_{\bar{\Theta}}$  in Eq. (5) with true  $\text{CH}_4$  concentration data). Due to the dataset being built on a restricted range of wind direction, the trained model is independent of the range direction is used for validation. Thus, for sources such as OSTPs (or other sources emitting  $\text{CH}_4$  from diluent degradation) the model can be used as a tool track emissions using  $\text{CH}_4$  concentration measurements from weather stations around them. For each year, we use our model to trace source emissions around each of the weather stations in consideration. Since abandoned ponds and EPLs are often ignored as sources, our goal is to monitored these tailings for emissions. While all ponds may not be equally active in emitting  $\text{CH}_4$ , the model suggests specific directions that need to be monitored as significant sources of emissions. A thorough analysis of emissions over four years shows that emissions from active OSTPs are not only increasing every year, some of the other inactive ponds/EPLs

such as WIP and Pond 5 could also be significant sources of CH<sub>4</sub> emissions. We found that the predicted emissions using our model were at least 20% more than the estimates in official reports [3, 15], where we consider the emission fraction from the reports based on Fine Fluid Tailings (FFT) volume of the OSTP. Other research works [26, 10] also support our evidence of emission under-reporting in the oil sands industry. Finally, We also used this model to compute the required level of emissions to reduce CH<sub>4</sub> concentrations in the region. It was found that in order to attain the target of atmospheric CH<sub>4</sub> concentrations around each weather, maximum emissions needed to be reduced from the direction of OSTPs. Building on the idea that emission reduction should also lead to reduced concentrations, it could take between 3-35% emission reduction to see improved air quality.

## 6 Conclusions

In this paper, we developed a constrained hybrid approach for predicting methane emissions and concentrations jointly. Our model formulation was based on learning the atmospheric methane concentrations using data obtained from weather monitoring stations subject to some physical constraints based on atmospheric dispersion models. We use a parameterized model to learn both, methane concentrations and the unknown functions in the constraints. Our input dataset included measurements from weather monitoring stations located within 4 km of active OSTPs and emission data obtained from solving different methanogenesis models. While our proposed framework can predict long term dynamics of concentrations and emissions as depicted in our simulations, there are some limitations that one must keep in mind while using this model. First, as discussed previously, the physical constraint may never be exactly satisfied. Secondly, due to absence of data regarding other methane emission sources (such as wetlands, industry emissions, etc.) our framework is limited to the sources selected for training (OSTPs in this study). As a part of future work, we plan to incorporate sources from all the wind directions into the framework by either using additional constraints based on existing mathematical models of various methane sources or by incorporating aspects of remote sensing to gather data of methane emissions around the OSTPs.

## Acknowledgements

The authors would like to acknowledge the and thank the Natural Sciences and Engineering Research Council of Canada (NSERC) for funding through an NSERC Alliance Missions grant on anthropogenic greenhouse gas research.

## Author contributions

**ES:** Writing: original draft, review and editing, Methodology, Investigation, Formal analysis, Supervision. **OW:** Writing: review and editing, Data curation, Investigation. **AKC:** Methodology, Data curation. **PVG:** Writing: review, Data curation, Formal analysis. **RM:** Writing: review, Funding acquisition. **HW:** Writing: review, Funding acquisition, Supervision, Project administration.

## Data availability

All data in this paper was obtained from other sources. This data will be available on request.

## Software

Softwares and packages used in the paper. **Python** version 3.6.8. **ArcGis Online**. All generated codes will be available post publication.

## Declaration of competing interest

The authors declare that there is no conflict of interest regarding the publication of this manuscript

## References

- [1] A. A. Abdel-Rahman. On the atmospheric dispersion and gaussian plume model. In *Proceedings of the 2nd International Conference on Waste Management, Water Pollution, Air Pollution, Indoor Climate, Corfu, Greece*, volume 26, 2008.
- [2] B. Adcock, S. Brugiapaglia, and C. G. Webster. *Sparse polynomial approximation of high-dimensional functions*, volume 25. SIAM, 2022.
- [3] Alberta Energy Regulator. 2022company-tailings-management-reports. <https://www.aer.ca>, 2022. Accessed: 2024-07-10.
- [4] Alberta Energy Regulator. Alberta mineable oil sands plant statistics. <https://www.aer.ca/providing-information/data-and-reports/statistical-reports/st39>, 2023. Accessed: 2024-05-10.
- [5] A. Andoni, R. Panigrahy, G. Valiant, and L. Zhang. Learning polynomials with neural networks. In *International conference on machine learning*, pages 1908–1916. PMLR, 2014.
- [6] K. Antonion, X. Wang, M. Raissi, and L. Joshie. Machine learning through physics-informed neural networks: Progress and challenges. *Academic Journal of Science and Technology*, 9(1):46–49, 2024.
- [7] R. Barratt. *Atmospheric dispersion modelling: an introduction to practical applications*. Routledge, 2013.
- [8] H. F. Bonifacio, R. G. Maghirang, E. B. Razote, S. L. Trabue, and J. H. Prueger. Comparison of aermod and windtrax dispersion models in determining pm10 emission rates from a beef cattle feedlot. *Journal of the Air & Waste Management Association*, 63(5):545–556, 2013.
- [9] Z. Burkus, J. Wheler, and S. Pletcher. Ghg emissions from oil sands tailings ponds: Overview and modelling based on fermentable substrates part i: Review of the tailings ponds facts and practices part ii: Modelling of ghg emissions from tailings ponds based on fermentable substrates zvonko burkus alberta environment and sustainable resource development (aesrd), 11 2014.
- [10] E. Chan, D. E. Worthy, D. Chan, M. Ishizawa, M. D. Moran, A. Delcloo, and F. Vogel. Eight-year estimates of methane emissions from oil and gas operations in western canada are nearly twice those reported in inventories. *Environmental Science & Technology*, 54(23):14899–14909, 2020.
- [11] A. Chkifa, A. Cohen, and C. Schwab. High-dimensional adaptive sparse polynomial interpolation and applications to parametric pdes. *Foundations of Computational Mathematics*, 14:601–633, 2014.
- [12] D. B. Das, S. K. Tatarwal, and R. Sharma. Release using dispersion modeling. *Quarterly Journal of the Hungarian Meteorological Service*, 102(3):167–187, 1998.
- [13] ECCC. Faster and further: Canada’s methane strategy. [https://publications.gc.ca/collections/collection\\_2022/eccc/En4-491-2022-eng.pdf](https://publications.gc.ca/collections/collection_2022/eccc/En4-491-2022-eng.pdf), 2022. Accessed: 2024-05-09.
- [14] M. D. Flannigan, M. A. Krawchuk, W. J. de Groot, B. M. Wotton, and L. M. Gowman. Implication of changing climate for global wildland fire. *International Journal of Wildland Fire*, 18(5):483–507, 2009.
- [15] Government of Alberta. Area fugitive emissions from oil sands mines. <https://open.alberta.ca/opendata/area-fugitive-emissions-from-oil-sands-mines>, 2022. Accessed: 2024-09-10.
- [16] S. Greydanus, M. Dzamba, and J. Yosinski. Hamiltonian neural networks. *Advances in neural information processing systems*, 32, 2019.
- [17] A. Hamrani, A. Akbarzadeh, and C. A. Madramootoo. Machine learning for predicting greenhouse gas emissions from agricultural soils. *Science of The Total Environment*, 741:140338, 2020.



- [18] A. Hashemi, H. Schaeffer, R. Shi, U. Topcu, G. Tran, and R. Ward. Generalization bounds for sparse random feature expansions. *Applied and Computational Harmonic Analysis*, 62:310–330, 2023.
- [19] L. Hu, C. Wang, Z. Ye, and S. Wang. Estimating gaseous pollutants from bus emissions: A hybrid model based on gru and xgboost. *Science of The Total Environment*, 783:146870, 2021.
- [20] C. C. Institute. Fact sheet: Early estimate of national emissions 2023. [https://climateinstitute.ca/wp-content/uploads/2024/09/Fact-sheet\\_Early-Estimate-of-National-Emissions-2023.pdf](https://climateinstitute.ca/wp-content/uploads/2024/09/Fact-sheet_Early-Estimate-of-National-Emissions-2023.pdf), September 19, 2024. Accessed: 2024-10-16.
- [21] G. E. Karniadakis, I. G. Kevrekidis, L. Lu, P. Perdikaris, S. Wang, and L. Yang. Physics-informed machine learning. *Nature Reviews Physics*, 3(6):422–440, 2021.
- [22] K. Kashinath, M. Mustafa, A. Albert, J. Wu, C. Jiang, S. Esmaeilzadeh, K. Azizzadenesheli, R. Wang, A. Chattopadhyay, A. Singh, et al. Physics-informed machine learning: case studies for weather and climate modelling. *Philosophical Transactions of the Royal Society A*, 379(2194):20200093, 2021.
- [23] J. D. Kong, H. Wang, T. Siddique, J. Foght, K. Semple, Z. Burkus, and M. A. Lewis. Second-generation stoichiometric mathematical model to predict methane emissions from oil sands tailings. *Science of the total environment*, 694:133645, 2019.
- [24] J. Li, H. Chen, T. Zhou, and X. Li. Tailings pond risk prediction using long short-term memory networks. *IEEE Access*, 7:182527–182537, 2019.
- [25] A. Liaw and M. Wiener. *randomForest: Breiman and Cutler’s Random Forests for Classification and Regression*, 2022. R package version 4.7-1.1.
- [26] J. Liggio, S.-M. Li, R. M. Staebler, K. Hayden, A. Darlington, R. L. Mittermeier, J. O’Brien, R. McLaren, M. Wolde, D. Worthy, et al. Measured canadian oil sands co2 emissions are higher than estimates made using internationally recommended methods. *Nature communications*, 10(1):1863, 2019.
- [27] R. Luo, J. Wang, and I. Gates. Machine learning for accurate methane concentration predictions: short-term training, long-term results. *Environmental Research Communications*, 5(8):081003, 2023.
- [28] W. S. McCulloch and W. Pitts. A logical calculus of the ideas immanent in nervous activity. *The bulletin of mathematical biophysics*, 5:115–133, 1943.
- [29] X. Meng, H. Chang, and X. Wang. Methane concentration prediction method based on deep learning and classical time series analysis. *Energies*, 15(6):2262, 2022.
- [30] T. Mikkelsen, S. Larsen, and H. Pécseli. Diffusion of gaussian puffs. *Quarterly Journal of the Royal Meteorological Society*, 113(475):81–105, 1987.
- [31] M. Mohan and T. Siddiqui. Development of an atmospheric dispersion model for air quality assessment. In *8th Int. Conf. on Harmonisation within Atmospheric Dispersion Modelling for Regulatory Purposes*, 2002.
- [32] NOAA National Centers for Environmental Information. Monthly global climate report for annual 2023. Technical report, National Oceanic and Atmospheric Administration, 2024.
- [33] T. Psomouli, I. Kansizoglou, and A. Gasteratos. Methane concentration forecasting based on sentinel-5p products and recurrent neural networks. *Geosciences*, 13(6):183, 2023.
- [34] A. Rahimi and B. Recht. Weighted sums of random kitchen sinks: Replacing minimization with randomization in learning. *Advances in neural information processing systems*, 21, 2008.

- [35] M. Raissi, P. Perdikaris, and G. E. Karniadakis. Physics-informed neural networks: A deep learning framework for solving forward and inverse problems involving nonlinear partial differential equations. *Journal of Computational physics*, 378:686–707, 2019.
- [36] E. Saha, L. S. T. Ho, and G. Tran. Spade4: Sparsity and delay embedding based forecasting of epidemics. *Bulletin of Mathematical Biology*, 85(8):71, 2023.
- [37] E. Saha, H. Schaeffer, and G. Tran. Harfe: hard-ridge random feature expansion. *Sampling Theory, Signal Processing, and Data Analysis*, 21(2):27, 2023.
- [38] H. Schaeffer, G. Tran, and R. Ward. Extracting sparse high-dimensional dynamics from limited data. *SIAM Journal on Applied Mathematics*, 78(6):3279–3295, 2018.
- [39] J. S. Scire, D. G. Strimaitis, R. J. Yamartino, et al. A user’s guide for the calpuff dispersion model. *Earth Tech, Inc*, 521:1–521, 2000.
- [40] T. Siddique, P. M. Fedorak, and J. M. Foght. Biodegradation of short-chain n-alkanes in oil sands tailings under methanogenic conditions. *Environmental Science & technology*, 40:5459–5464, 2006.
- [41] T. Siddique, P. M. Fedorak, M. D. MacKinnon, and J. M. Foght. Metabolism of btex and naphtha compounds to methane in oil sands tailings. *Environmental Science & technology*, 41:2350–2356, 2007.
- [42] T. Siddique, R. Gupta, P. M. Fedorak, M. D. MacKinnon, and J. M. Foght. A first approximation kinetic model to predict methane generation from an oil sands tailings settling basin. *Chemosphere*, 72(10):1573–1580, 2008.
- [43] J. Solano, T. Montaña, J. Maldonado-Correa, A. Ordóñez, and M. Pesantez. Correlation between the wind speed and the elevation to evaluate the wind potential in the southern region of ecuador. *Energy Reports*, 7:259–268, 2021.
- [44] J. M. Stockie. The mathematics of atmospheric dispersion modeling. *Siam Review*, 53(2):349–372, 2011.
- [45] L. Sysoeva, I. Bouderbala, M. H. Kent, E. Saha, B. A. Zambrano-Luna, R. Milne, and H. Wang. Decoding methane concentration in alberta oil sands: a machine learning exploration. *Unpublished, currently under review*, 2024.
- [46] F. Tagliaferri, M. Invernizzi, F. Capra, and S. Sironi. Validation study of windtrax reverse dispersion model coupled with a sensitivity analysis of model-specific settings. *Environmental research*, 222:115401, 2023.
- [47] F. Tagliaferri, M. Invernizzi, S. Sironi, et al. Validation study of windtrax backward lagrangian model. In *Harmo 21 Proceedings*, pages 463–468. Universidade de Aveiro, 2022.
- [48] W. Tong, L. Li, X. Zhou, A. Hamilton, and K. Zhang. Deep learning pm 2.5 concentrations with bidirectional lstm rnn. *Air Quality, Atmosphere & Health*, 12:411–423, 2019.
- [49] D. B. Turner. *Workbook of atmospheric dispersion estimates: an introduction to dispersion modeling*. CRC press, 2020.
- [50] US EPA. Overview of greenhouse gases. <https://www.epa.gov/ghgemissions/overview-greenhouse-gases#methane>, 2024. Accessed: 2024-05-09.
- [51] P. Venegas Garcia, A. K. Luznetsova, T. Siddique, and H. Wang. Temperature-dependent mechanistic model to predict methane biogenesis from an oil sands tailings settling basin. *Unpublished, manuscript under preparation*, 2024.
- [52] Wood Buffalo Enviornmental Association. Network map & station data. <https://wbea.org/data/network-map-station-data/>, Accessed: 2024-05-15.

- [53] X. Wu et al. Image extraction of tailings pond guided by artificial intelligence support vector machine. *Wireless Communications and Mobile Computing*, 2022, 2022.
- [54] H. Xie, L. Ji, Q. Wang, and Z. Jia. Research of pm2. 5 prediction system based on cnns-gru in wuxi urban area. In *IOP Conference Series: Earth and Environmental Science*, volume 300, page 032073. IOP Publishing, 2019.
- [55] K. Xu and E. Darve. Physics constrained learning for data-driven inverse modeling from sparse observations. *Journal of Computational Physics*, 453:110938, 2022.
- [56] J. Yang, Y. Sun, Q. Li, and Y. Sun. Effective risk prediction of tailings ponds using machine learning. In *2020 3rd International Conference on Advanced Electronic Materials, Computers and Software Engineering (AEMCSE)*, pages 234–238. IEEE, 2020.
- [57] H. Yu and I. Zahidi. Tailings pond classification based on satellite images and machine learning: An exploration of microsoft ml. net. *Mathematics*, 11(3):517, 2023.